EUROPEAN ORGANIZATION FOR NUCLEAR RESEARCH (CERN)

CERN-EP-2022-032
2022/07/05

CMS-SUS-21-001

Search for direct pair production of supersymmetric partners of τ leptons in the final state with two hadronically decaying τ leptons and missing transverse momentum in proton-proton collisions at $\sqrt{s} = 13\,\text{TeV}$

The CMS Collaboration

Abstract

A search for the direct production of a pair of τ sleptons, the supersymmetric partners of τ leptons, is presented. Each τ slepton is assumed to decay to a τ lepton and the lightest supersymmetric particle (LSP), which is assumed to be stable and to not interact in the detector, leading to an imbalance in the total reconstructed transverse momentum. The search is carried out in events identified as containing two τ leptons, each decaying to one or more hadrons and a neutrino, and significant transverse momentum imbalance. In addition to scenarios in which the τ sleptons decay promptly, the search also addresses scenarios in which the τ sleptons have sufficiently long lifetimes to give rise to nonprompt τ leptons. The data were collected in proton-proton collisions at a center-of-mass energy of 13 TeV at the CERN LHC with the CMS detector in 2016–2018, and correspond to an integrated luminosity of $138\,\text{fb}^{-1}$. No significant excess is seen with respect to standard model expectations. Upper limits on cross sections for the pair production of τ sleptons are obtained in the framework of simplified models. In a scenario in which the τ sleptons are superpartners of left-handed τ leptons, and each undergoes a prompt decay to a τ lepton and a nearly massless LSP, τ slepton masses between 115 and 340 GeV are excluded. In a scenario in which the lifetime of the τ sleptons corresponds to $c\tau_0 = 0.1\,\text{mm}$, where τ_0 represents the mean proper lifetime of the τ slepton, masses between 150 and 220 GeV are excluded.

Submitted to Physical Review D

1 Introduction

Supersymmetry (SUSY) [1–8] is appealing because it could address some of the shortcomings of the standard model (SM) of particle physics. It features superpartners, i.e., new particles with the same quantum numbers as their SM counterparts, with the exception of their spin, which is shifted by half a unit. The superpartner loop contributions in the radiative corrections to the Higgs boson mass could cancel quadratic divergences, thus solving the fine-tuning problem [9–12]. In SUSY models with R-parity conservation [13], the lightest supersymmetric particle (LSP) is stable and could be a dark matter (DM) candidate [14–16].

In this paper, we report the results of a search for the τ slepton ($\widetilde{\tau}$), the superpartner of the τ lepton, in proton-proton (pp) collisions at a center-of-mass energy of 13 TeV, with the CMS detector. Early universe $\widetilde{\tau}$-neutralino coannihilation models provide a mechanism that can explain the observed DM relic density [17–22]. These models motivate the existence of a light $\widetilde{\tau}$ as the next-to-lightest supersymmetric particle (NLSP), which would lead to an enhanced rate of production of final states with τ leptons in collider experiments [23, 24]. Here, we study events with two τ lepton candidates, both undergoing hadronic decays (τ_{h}), and having significant transverse momentum imbalance resulting from the presence of LSPs and to a lesser extent, neutrinos from the τ lepton decays. While previous searches in this final state have largely focused on prompt decays of the parent particles, the present search also addresses scenarios in which the $\widetilde{\tau}$ is long-lived, which can arise in theories of gauge-mediated SUSY breaking (GMSB) that in many cases predict a $\widetilde{\tau}$ as the NLSP [25]. This search is the first to target final states in which reconstructed τ_{h} candidates are identified as having production vertices that are significantly displaced from the primary interaction point as expected for long-lived $\widetilde{\tau}$ decays.

Figure 1 shows a diagram of direct $\widetilde{\tau}$ pair production, with the $\widetilde{\tau}$ decaying to a τ lepton and LSP, which we study in this paper within the framework of simplified models [26–28]. For models featuring prompt decays of the $\widetilde{\tau}$, we assume $\widetilde{\chi}_1^0$, the lightest neutralino, to be the LSP, and consider a range of $\widetilde{\chi}_1^0$ masses up to 200 GeV. We use the symbols $\widetilde{\tau}_{\mathrm{L}}$ and $\widetilde{\tau}_{\mathrm{R}}$ to refer to the superpartners of left- and right-handed τ leptons, respectively. We consider cases in which only $\widetilde{\tau}_{\mathrm{L}}$ or only $\widetilde{\tau}_{\mathrm{R}}$ pairs are produced, as well as a degenerate case in which both $\widetilde{\tau}_{\mathrm{L}}$ and $\widetilde{\tau}_{\mathrm{R}}$ pairs are produced. The cross section for $\widetilde{\tau}_{\mathrm{L}}$ pair production is expected to be approximately three times larger than for $\widetilde{\tau}_{\mathrm{R}}$ pair production [29], while the experimental acceptance is expected to be higher in the right-handed case than in the left-handed because of differences in the polarization of the τ leptons that are produced. The small production cross section expected for the signal and the significant SM backgrounds make this search challenging.

Previous searches for direct $\widetilde{\tau}$ pair production in prompt decay scenarios were performed at the CERN LEP collider [30–33] and excluded $\widetilde{\tau}$ masses at 95% confidence level (CL) up to about 90 GeV for neutralino masses up to 80 GeV, in some models. The ATLAS [34, 35] and CMS [36] Collaborations performed searches for direct $\widetilde{\tau}$ pair production using 8 TeV CERN LHC data. The ATLAS Collaboration has reported the results of a search for direct $\widetilde{\tau}$ pair production using 13 TeV data corresponding to an integrated luminosity of 139 fb^{-1} [37] that excludes $\widetilde{\tau}$ masses between 155 and 310 GeV at 95% CL, for the case of a nearly massless LSP. The CMS Collaboration has previously reported the results of a search for direct $\widetilde{\tau}$ pair production using data collected in 2016–2017 at $\sqrt{s} = 13$ TeV, corresponding to an integrated luminosity of 77.2 fb^{-1} [38], and placed upper limits on the cross section for $\widetilde{\tau}$ pair production.

We also target scenarios where the $\widetilde{\tau}$ has a short but finite lifetime, decaying within a few cm of the primary interaction point. These signatures are sensitive to GMSB SUSY models in which

a nearly massless gravitino ($\widetilde{\mathrm{G}}$) is the LSP and the $\widetilde{\tau}$ is the NLSP that can become long-lived as a result of its suppressed coupling to the gravitino. We consider models involving the pair production of $\widetilde{\tau}_1$, a mixture of $\widetilde{\tau}_\mathrm{L}$ and $\widetilde{\tau}_\mathrm{R}$, for $c\tau_0$ up to 2.5 mm, where τ_0 is the mean proper lifetime of the $\widetilde{\tau}_1$. For these models, we assume a scenario with maximal mixing, i.e., with a mixing angle of $\frac{\pi}{4}$, for which the cross section is very similar to that for purely right-handed $\widetilde{\tau}$ pair production [29]. This scenario is therefore consistent with GMSB SUSY models, in which the $\widetilde{\tau}$ is typically right-handed. Previously, the LEP experiments set limits on GMSB SUSY models with $\widetilde{\tau}_1$ as the NLSP, with the strongest limits coming from the OPAL experiment [39]. The OPAL limits excluded masses up to 87.4 GeV at 95% CL, for all $\widetilde{\tau}_1$ lifetimes. The ATLAS Collaboration recently reported the results of a search for long-lived sleptons, including $\widetilde{\tau}_{1,2}$, a combination of mixed states of $\widetilde{\tau}_\mathrm{L}$ and $\widetilde{\tau}_\mathrm{R}$, in final states with nonprompt electrons or muons. The degenerate production of the two mixed states $\widetilde{\tau}_1$ and $\widetilde{\tau}_2$ results in a larger cross section than the production of $\widetilde{\tau}_1$ alone. The search excluded $\widetilde{\tau}_{1,2}$ masses up to 340 GeV for a proper lifetime of 0.1 ns, i.e., for a $c\tau_0$ of 30 mm, within the simplified GMSB SUSY model considered [40], under the assumption of a nearly massless LSP.

The results presented in this paper supersede those of the search reported in Ref. [38], for final states with two τ_h candidates and missing transverse momentum ($p_\mathrm{T}^\mathrm{miss}$), and also include scenarios with long-lived τ sleptons. The LHC pp collision data collected with the CMS detector in 2018 have been analyzed, and the data collected in 2016–2017 have been re-analyzed, resulting in a sample corresponding to a total integrated luminosity of 138 fb^{-1}. Improved techniques are used to describe the SM background with τ leptons through a method called "embedding" [41], which estimates the background with two genuine τ lepton candidates by selecting dimuon events in data, removing reconstructed muons, and replacing them with simulated τ lepton decays. Updated methods are used for the τ_h candidate selection [42] and the search region definitions have been re-optimized. Overall, we obtain a significant improvement in the search sensitivity. Tabulated results are provided in the HEPData record for this analysis [43].

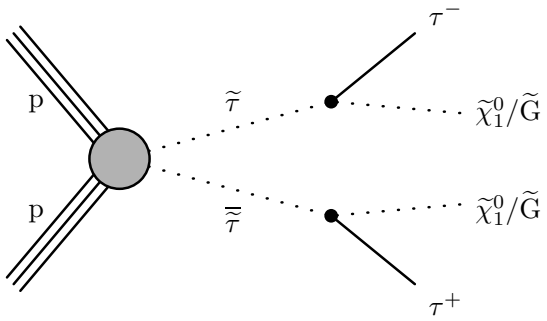

Figure 1: Diagram for direct $\widetilde{\tau}$ pair production, followed by decay of each $\widetilde{\tau}$ to a τ lepton and an LSP. For models with promptly decaying τ sleptons, the LSP is assumed to be $\widetilde{\chi}_1^0$, the lightest neutralino. For models with long-lived τ sleptons, it is assumed to be the gravitino, $\widetilde{\mathrm{G}}$.

2 The CMS detector

The central feature of the CMS apparatus is a superconducting solenoid of 6 m internal diameter, providing a magnetic field of 3.8 T. A silicon pixel and strip tracker, a lead tungstate crystal electromagnetic calorimeter, and a brass and scintillator hadron calorimeter, each composed of a barrel and two endcap sections, reside within the solenoid volume. Forward calorimeters

extend the pseudorapidity (η) coverage provided by the barrel and endcap detectors. Muons are detected in gas-ionization chambers embedded in the steel flux-return yoke outside the solenoid. Events of interest are selected using a two-tiered trigger system. The first level (L1), composed of custom hardware processors, uses information from the calorimeters and muon detectors to select events at a rate of around 100 kHz within a fixed latency of about 4 μs [44]. The second level, known as the high-level trigger (HLT), consists of a farm of processors running a version of the full event reconstruction software optimized for fast processing, and reduces the event rate to around 1 kHz before data storage [45].

3 Event reconstruction and simulation

The event reconstruction uses the particle-flow (PF) algorithm [46], which aims to reconstruct and identify individual particles in an event, with an optimized combination of information from the various elements of the CMS detector. The vector $\vec{p}_{\mathrm{T}}^{\,\mathrm{miss}}$ is computed as the negative vector sum of the transverse momenta, $\vec{p}_{\mathrm{T}}$, of all PF-reconstructed particles in an event. Its magnitude, $p_{\mathrm{T}}^{\mathrm{miss}}$, is used in the search as a discriminator between signal and SM background. Events selected for the search are required to pass selection criteria [47] designed to remove anomalous high-$p_{\mathrm{T}}^{\mathrm{miss}}$ events that can occur due to a variety of reconstruction failures, detector malfunctions, or noncollision backgrounds, and must have at least one reconstructed pp interaction vertex. The primary vertex (PV) is taken to be the vertex corresponding to the hardest scattering in the event, evaluated using tracking information alone, as described in Section 9.4.1 of Ref. [48].

Reconstructed particles are clustered into jets using the anti-k_{T} algorithm [49, 50] with a distance parameter of 0.4. Jet momentum is determined as the vectorial sum of all particle momenta in the jet, and is found from simulation to be, on average, within 5 to 10% of the true momentum over the whole p_{T} spectrum and detector acceptance. Additional pp interactions within the same or nearby bunch crossings (pileup) can contribute additional tracks and calorimetric energy depositions, increasing the apparent jet momentum. To mitigate this effect, tracks identified to be originating from pileup vertices are discarded and an offset correction is applied to correct for remaining contributions. Jet energy corrections are derived from simulation studies so that the average measured energy of jets becomes identical to that of particle level jets. In situ measurements of the momentum balance in dijet, photon+jet, Z+jet, and multijet events are used to determine any residual differences between the jet energy scale in data and in simulation, and appropriate corrections are made [51]. Jets considered in this analysis, other than those from which τ_{h} candidates are reconstructed, are required to be within the tracker volume, $|\eta| < 2.4$, and to satisfy the condition $p_{\mathrm{T}} > 30\,\mathrm{GeV}$. They are required to be separated in the plane of η and azimuthal angle (ϕ) by $\Delta R \equiv \sqrt{(\Delta\eta)^2 + (\Delta\phi)^2} > 0.4$ from τ_{h} candidates to avoid the double counting of objects. The deep neural network (DNN) based combined secondary vertex algorithm (DEEPCSV) [52] is used to identify, or "tag", jets originating from the hadronization of b quarks. A high-efficiency ("Loose") working point of this algorithm is used to reject events with b quark jets that are likely to have originated from SM backgrounds with top quarks. This working point corresponds to an efficiency of $\approx$84% for identifying b quarks originating from top quark decays, and misidentification rates of about 41 and 11%, respectively, for jets from charm quarks and from light quarks or gluons.

In order to suppress SM backgrounds, such as those originating from diboson production, or $\mathrm{t\bar{t}}$ production in association with a vector boson, we veto events with isolated electron or muon candidates. We identify these charged leptons using the same selection criteria as those described in [38]. The τ_{h} candidates are reconstructed from jets, using the hadrons-plus-strips

algorithm [53], which combines 1 or 3 tracks with energy deposits in the calorimeters, to identify the τ_h decay modes. Decay modes with one or three charged hadrons, with or without neutral pions, are considered in this search. To distinguish genuine τ_h decays from electrons, muons, or jets originating from the hadronization of quarks or gluons, the multi-class DNN-based DEEPTAU [42] algorithm is used. Information from all individual reconstructed particles near the τ_h axis is combined with properties of the τ_h candidate and event activity. We employ both a relaxed ("Loose") and a more stringent ("VVTight") working point of the anti-jet DEEPTAU discriminant. These have efficiencies of ≈80 and ≈40% for a genuine τ_h decay in the case of prompt τ_h production, respectively, and misidentification rates of ≈0.5 and ≈0.06%, respectively, for quark and gluon jets. Since the DEEPTAU algorithm was optimized for promptly produced τ_h candidates, the efficiency is reduced in the case of τ_h candidates originating from long-lived τ slepton decays. The efficiency of the "VVTight" working point, which is used to select signal τ_h candidates, ranges between 20% and 30% for the largest $\widetilde{\tau}$ lifetimes considered in the search regions that explicitly target displaced τ_h decays.

Monte Carlo (MC) simulation is used to model the signal. The MADGRAPH5_aMC@NLO version 2.3.3 and 2.4.2 event generators [54] are used at leading order (LO) precision to generate models of direct $\widetilde{\tau}$ pair production for promptly decaying $\widetilde{\tau}$ up to the production of τ leptons, for simulated event samples corresponding to the 2016 and 2017–2018 data sets, respectively. The τ lepton decays are modeled by PYTHIA 8.2 (8.212 for 2016, or 8.230 for 2017–2018) [55]. For signal models in which the $\widetilde{\tau}$ undergoes nonprompt decays, the $\widetilde{\tau}$ pair production process is generated with MADGRAPH5_aMC@NLO at LO precision, with the $\widetilde{\tau}$ decays being subsequently carried out by PYTHIA, using a specified $\widetilde{\tau}$ lifetime. We consider models with $c\tau_0$ ranging from 0.01 to 2.5 mm. In the case of both prompt and long-lived τ sleptons, we consider $\widetilde{\tau}$ masses ranging from 90 to 500 GeV. The CUETP8M1 underlying event tune [56] is used with PYTHIA for simulated event samples corresponding to the 2016 data set, and the CP5 tune [57] is used for 2017 and 2018 samples. The NNPDF3.0LO [58] set of parton distribution functions (PDFs) is used in generating the 2016 simulation samples, while the NNPDF3.1 next-to-leading order (NLO) PDFs are used for 2017–2018. Showering and hadronization of partons are carried out using PYTHIA, while a detailed simulation of the CMS detector is based on the GEANT4 [59] package. Finally, uncertainties in the renormalization and factorization scales have been obtained using the SYSCALC package [60]. The signal production cross sections are calculated at NLO using next-to-leading logarithmic (NLL) soft-gluon resummation [29].

We also use MC simulation to model the background from SM production of Higgs bosons. The POWHEGv2 [61–64] generator is used to produce samples of Higgs boson events with decays to τ lepton pairs. Other backgrounds, originating from processes that give rise to two genuine τ_h decays, or to one or more jets that are misidentified as τ_h candidates, are estimated from data, as described in Section 5. The background from events in which an electron or muon is misidentified as a τ_h candidate is found from simulation to be negligible.

Simulated events are weighted to match the pileup profile observed in data. Scale factors are applied to simulated events to account for differences with respect to data in trigger efficiencies, τ_h identification efficiencies, jet and τ_h energy scales, and b tagging efficiency. We improve the modeling of initial-state radiation (ISR) in the 2016 signal simulation samples by reweighting the p_T^{ISR} distribution, where p_T^{ISR} corresponds to the magnitude of the total transverse momentum of the system of parent SUSY particles, obtained in our case by calculating the vector sum of the p_T of the two τ sleptons at generator level. This reweighting procedure is based on studies of the p_T of Z bosons in data and simulation [65]. No corrections were found to be necessary for the p_T^{ISR} distribution in 2017 and 2018 simulation samples, as the ISR modeling was improved in the simulation with the updated underlying-event tune.

4 Event selection

The data used in this search are selected with two sets of triggers: a trigger requiring the presence of two τ_h candidates, each with $p_T > 35$ (>40) GeV in 2016 (2017–2018) data, and a p_T^{miss}-based trigger, with a threshold varying between 100 and 140 GeV, depending on the data-taking period. The di-τ_h trigger is used for events with $p_T^{miss} < 200$ GeV, while the p_T^{miss}-based trigger is used for events with $p_T^{miss} > 200$ GeV. The offline p_T^{miss} threshold is chosen to be close to the range in which the efficiency of the p_T^{miss}-based trigger reaches its plateau.

After the trigger selection, we impose a baseline event selection requiring the presence of exactly two τ_h candidates of opposite charge with $p_T > 40$ GeV, $|\eta| < 2.1$, and satisfying the "VVTight" DEEPTAU selection and other criteria described in Section 3. Backgrounds originating from diboson production or $t\bar{t}$ production in association with a vector boson are suppressed by vetoing events with electron or muon candidates with $p_T > 20$ GeV and $|\eta| < 2.5$ or <2.4 for electrons and muons respectively, or additional τ_h candidates with $p_T > 30$ GeV satisfying the "Loose" DEEPTAU selection. We reject any events with a b-tagged jet to suppress top quark backgrounds, and we require $|\Delta\phi(\tau_h^{(1)}, \tau_h^{(2)})| > 1.5$. This requirement retains high signal efficiency while reducing the background from $Z/\gamma^* \to \tau\tau$+jets events in which the di-τ_h system is boosted, resulting in a smaller angular separation between the τ_h candidates. Finally, we require $p_T^{miss} > 50$ GeV to suppress the background with two misidentified τ_h candidates. To avoid effects related to jet mismeasurement that can contribute to spurious p_T^{miss}, we require the $\vec{p}_T^{miss}$ to have a minimum separation of 0.25 in $|\Delta\phi|$ from reconstructed jets.

The search strategy relies on a simultaneous maximum likelihood fit of the event yields observed in 31 search regions (SRs), which are described below and summarized in Table 1. We use a number of discriminants to subdivide events satisfying the baseline selection criteria into exclusive SRs. For signal events, we expect the two stable LSPs in the final state to contribute to the p_T^{miss}. Consequently, we expect the correlations between $\vec{p}_T^{miss}$ and the reconstructed τ_h candidates to be different between signal and background events. Mass observables calculated from $\vec{p}_T^{miss}$ and the p_T of the τ_h can be used to exploit these differences and discriminate signal from background.

One of the discriminants used is Σm_T, the sum of the transverse masses (m_T) calculated for each τ_h candidate with p_T^{miss}, given by

$$\Sigma m_T = m_T(\tau_h^{(1)}) + m_T(\tau_h^{(2)}), \tag{1}$$

where the transverse mass for each τ_h candidate is

$$m_T(\tau_h) \equiv \sqrt{2 p_T^{\tau_h} p_T^{miss} [1 - \cos\Delta\phi(\vec{p}_T^{\tau_h}, \vec{p}_T^{miss})]}. \tag{2}$$

For our signal models, p_T^{miss} can originate from neutrinos from τ_h decays, as well as from LSPs. However, the predominant contribution to the p_T^{miss} is expected to come from the LSPs, which we assume to be massless in the calculation of m_T.

We also use the "stransverse mass" m_{T2} [66–68], given by

$$m_{T2} = \min_{\vec{p}_T^{X(1)} + \vec{p}_T^{X(2)} = \vec{p}_T^{miss}} \left[\max\left(m_T^{(1)}, m_T^{(2)} \right) \right], \tag{3}$$

where $\vec{p}_T^{X(i)}$ (with i=1, 2) are the unknown transverse momenta of the two invisible particles, X(1) and X(2), corresponding to the LSPs in our signal models, and $m_T^{(i)}$ are the transverse

masses calculated from the assigned LSP transverse momenta. The latter are obtained by associating either of the two LSPs, assumed to be massless, to one of the two parent $\widetilde{\tau}$ decays. The minimization of Eq. (3) is performed over all possible LSP 3-vector momenta, which are constrained to add up to the $\vec{p}_{\mathrm{T}}^{\,\mathrm{miss}}$ in the event. We expect large values of m_{T2} to occur more frequently in signal events for models with larger $\widetilde{\tau}$ masses, and to occur relatively rarely in SM background events.

For the selection of events in the SRs, requirements of $m_{\mathrm{T2}} > 25\,\mathrm{GeV}$ and $\Sigma m_{\mathrm{T}} > 200\,\mathrm{GeV}$ are imposed. Two sets of SRs are defined: the "prompt" SRs, targeting models in which the $\widetilde{\tau}$ decays promptly, and the "displaced" SRs, targeting long-lived $\widetilde{\tau}$ models in which nonprompt τ_{h} candidates are expected.

In order to ensure that the prompt and displaced SRs are disjoint, we require that events in the prompt SRs have at least one τ_{h} that does not satisfy the "displaced τ_{h}" criteria described below for the displaced SRs. Events are then subdivided into bins of m_{T2} and Σm_{T}, which provides sensitivity to a range of $\widetilde{\tau}$ masses. We further subdivide events into two categories based on the number of reconstructed jets (N_{j}): $N_{\mathrm{j}} = 0$, and $N_{\mathrm{j}} \geq 1$. Since background events that satisfy the SR kinematic selection criteria usually contain additional jets, the 0–jet category provides SRs with improved signal-to-background ratios. Signal events with ISR or pileup jets may populate the $N_{\mathrm{j}} \geq 1$ SRs, and so we also retain these to avoid losing signal sensitivity. Finally, we gain additional sensitivity in bins with lower Σm_{T} and m_{T2} values ($\Sigma m_{\mathrm{T}} < 300\,\mathrm{GeV}$ and $m_{\mathrm{T2}} < 75\,\mathrm{GeV}$) in the 0–jet category, which have relatively high background, by further subdividing them into two bins based on the p_{T} of the leading (higher-p_{T}) τ_{h} candidate, $p_{\mathrm{T}}^{\tau_{\mathrm{h},1}}$ ($p_{\mathrm{T}}^{\tau_{\mathrm{h},1}} < 90\,\mathrm{GeV}$, and $p_{\mathrm{T}}^{\tau_{\mathrm{h},1}} \geq 90\,\mathrm{GeV}$). This further improves the discrimination of signal from background as τ_{h} in signal events tend to have higher p_{T}.

The displaced category is defined by imposing the following "displaced τ_{h}" criteria for both τ_{h} candidates. We require the significance of the τ_{h} impact parameter relative to the PV in the transverse plane (d_{xy}), defined as the quantity divided by its uncertainty, to have an absolute value above 5, and the absolute value of its three-dimensional impact parameter (IP3D) to exceed $100\,\mu\mathrm{m}$. We also require $|\Delta\phi(\tau_{\mathrm{h}}^{(1)}, \tau_{\mathrm{h}}^{(2)})| > 1.75$ to further suppress the background in the displaced category. For events satisfying these selection criteria, the p_{T} of the subleading (lower-p_{T}) τ_{h} candidate, $p_{\mathrm{T}}^{\tau_{\mathrm{h},2}}$, provides additional discrimination between signal and the remaining background. Accordingly, we define two SR bins for events in this category, with $p_{\mathrm{T}}^{\tau_{\mathrm{h},2}} < 110\,\mathrm{GeV}$ and $p_{\mathrm{T}}^{\tau_{\mathrm{h},2}} \geq 110\,\mathrm{GeV}$.

The SR binning was chosen to optimize the search sensitivity, with statistical and systematic uncertainties in the signal and background predictions being taken into account in the optimization procedure. Table 1 summarizes the Σm_{T}, m_{T2}, and $p_{\mathrm{T}}^{\tau_{\mathrm{h},1}}$ criteria used to define the prompt SRs, and the $p_{\mathrm{T}}^{\tau_{\mathrm{h},2}}$ criteria used to define the displaced SRs. Figure 2 shows distributions of Σm_{T}, m_{T2}, and $p_{\mathrm{T}}^{\tau_{\mathrm{h},1}}$ for events satisfying the selection criteria that are common to all prompt SRs in data, along with the corresponding background estimates that are obtained using the methods described in Section 5. Predicted signal distributions are shown for three benchmark models of purely left-handed $\widetilde{\tau}$ pair production with prompt decays with $\widetilde{\tau}_{\mathrm{L}}$ masses of 100, 150, and 200 GeV and an LSP mass of 1 GeV. The distribution of $p_{\mathrm{T}}^{\tau_{\mathrm{h},2}}$ is also shown for events satisfying the common selection criteria of the displaced SRs for data, the predicted background, and two benchmark models of long-lived $\widetilde{\tau}$ pair production in the maximally-mixed scenario ($\widetilde{\tau}_{\mathrm{MM}}$) with a $\widetilde{\tau}_{\mathrm{MM}}$ mass of 150 GeV, an LSP mass of 1 GeV, and $c\tau_0$ values of 0.5 and 1 mm.

Table 1: Ranges of Σm_{T}, m_{T2}, and $p_{\mathrm{T}}^{\tau_{\mathrm{h},1}}$ used to define the prompt SRs for the $N_{\mathrm{j}} = 0$ and $N_{\mathrm{j}} \geq 1$ event categories, and ranges of $p_{\mathrm{T}}^{\tau_{\mathrm{h},2}}$ used to define the displaced SRs.

Prompt SRs			
SR bin	Σm_{T} [GeV]	m_{T2} [GeV]	$p_{\mathrm{T}}^{\tau_{\mathrm{h},1}}$ [GeV]
$N_{\mathrm{j}} = 0$			
1	$200-250$	$25-50$	<90
2	$200-250$	$25-50$	>90
3	$200-250$	$50-75$	<90
4	$200-250$	$50-75$	>90
5	$200-250$	>75	—
6	$250-300$	$25-50$	<90
7	$250-300$	$25-50$	>90
8	$250-300$	$50-75$	<90
9	$250-300$	$50-75$	>90
10	$250-300$	>75	—
11	$300-350$	$25-50$	—
12	$300-350$	$50-75$	—
13	$300-350$	$75-100$	—
14	$300-350$	>100	—
15	>350	$25-50$	—
16	>350	$50-75$	—
17	>350	$75-100$	—
18	>350	>100	—
$N_{\mathrm{j}} \geq 1$			
19	$200-250$	$25-50$	—
20	$200-250$	>50	—
21	$250-300$	$25-50$	—
22	$250-300$	$50-75$	—
23	$250-300$	>75	—
24	$300-350$	$25-50$	—
25	$300-350$	$50-75$	—
26	$300-350$	>75	—
27	>350	$25-75$	—
28	>350	$75-100$	—
29	>350	>100	—
Displaced SRs			
SR bin	$p_{\mathrm{T}}^{\tau_{\mathrm{h},2}}$ [GeV]		
30	<110		
31	>110		

5 Background estimation

Significant contributions to the SM background in this search originate from $\mathrm{Z}/\gamma^* \to \tau\tau$+jets, W+jets, $\mathrm{t\bar{t}}$, and diboson processes, as well as from events exclusively comprising jets produced through the strong interaction of quantum chromodynamics (QCD), which we refer to as QCD multijet events. Smaller contributions arise from single top quark production and rare SM processes, such as triboson and Higgs boson production, and top quark pair production in association with vector bosons. We rely on a method based on control samples in data to estimate the contributions of backgrounds in which one or both τ_{h} candidates are misidentified jets.

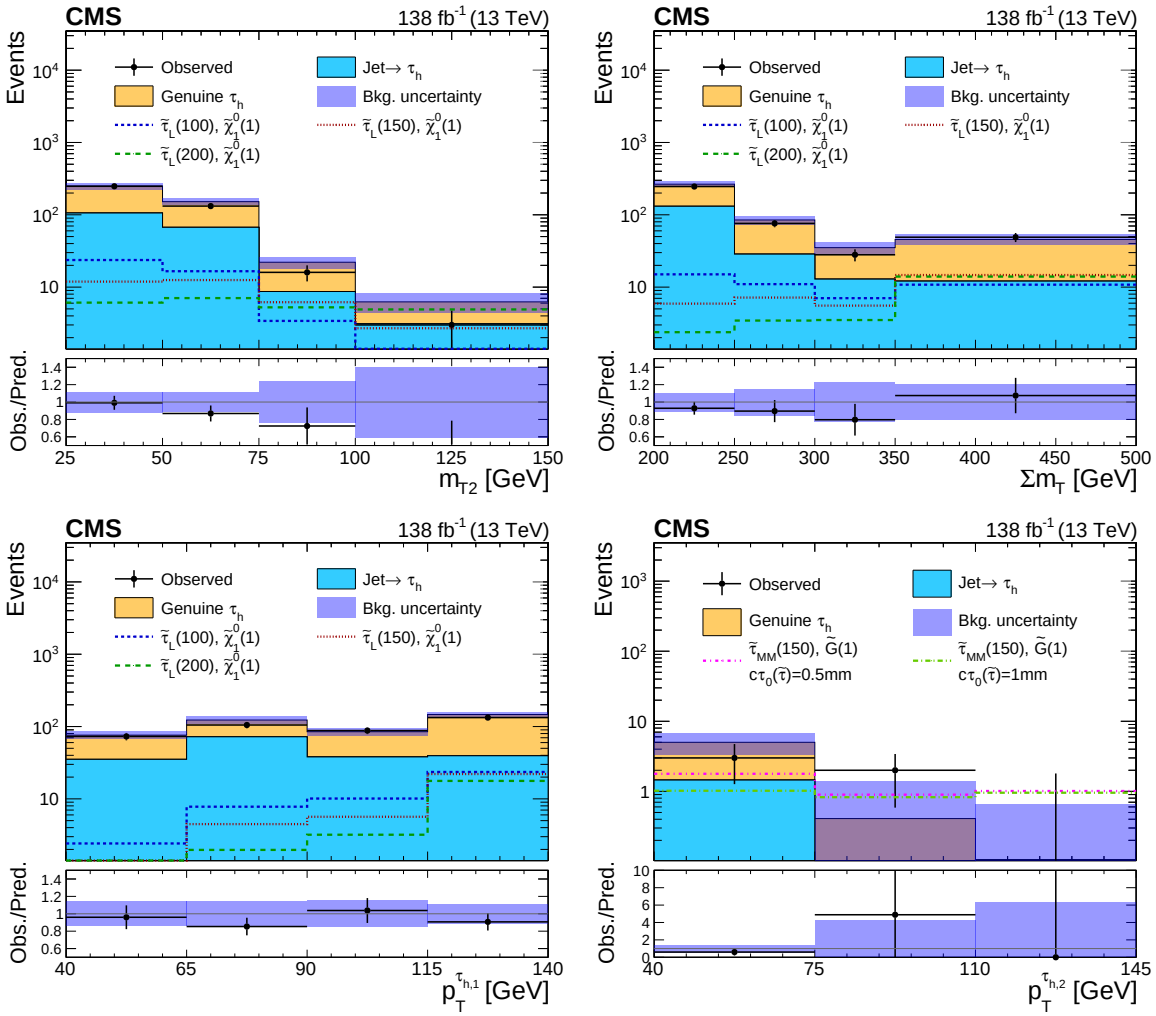

Figure 2: Distributions of m_{T2} (upper left), Σm_{T} (upper right), and $p_{\mathrm{T}}^{\tau_{\mathrm{h},1}}$ (lower left) for events passing the selection criteria common to all prompt SRs, and of $p_{\mathrm{T}}^{\tau_{\mathrm{h},2}}$ (lower right) for those passing the criteria common to all displaced SRs. The shaded band indicates the combined statistical and systematic uncertainty in the total SM background prediction. The lower panels show the ratio of the observed event counts to the total background prediction. Signal distributions are shown for benchmark models of $\widetilde{\tau}$ pair production that are described in the text. The numbers in parentheses correspond to the masses of the $\widetilde{\tau}$ and LSP in units of GeV for the different signal models.

Contributions from backgrounds with electrons or muons misidentified as τ_{h} candidates are negligible. We use a method known as "embedding" for modeling backgrounds with two genuine τ_{h} decays [41], which has the advantage that many event quantities are described by data. The background estimation methods described below are validated in dedicated background-enriched data samples that are similar in many respects but disjoint to the SRs. Separate samples are used to validate the modeling of backgrounds with prompt and displaced τ_{h} candidates.

5.1 Estimation of background from misidentified jets

Events with misidentified τ_{h} candidates, originating predominantly from QCD multijet and W+jets production, constitute the dominant background after the requirement of two τ_{h} candi-

dates with high p_T. We estimate this background by extrapolating the event count in a control data sample into the SR, following the same approach as that described in [38]. The control sample is selected with a relaxed τ_h identification requirement, namely the Loose working point of the DEEPTAU discriminant. We measure the fraction of misidentified τ_h candidates selected with the Loose working point that also satisfy the VVTight requirement in a QCD multijet-enriched sample of same-charge $\tau_h\tau_h$ events. The fraction is found to be ≈10–15%, and depends on the p_T and decay mode of the τ_h candidate, as well as on the additional activity in an event from the presence of pileup. We parameterize the measurement by the p_T and decay mode of the τ_h candidate as well as the number of reconstructed primary vertices to take these effects into account. The misidentification rate also depends on the jet flavor, i.e., whether the misidentified jet originates from the hadronization of light- or heavy-flavor quarks, or gluons, which cannot be reliably determined in data. We assign a systematic uncertainty of 30% based on studies of the variation of the misidentification rate with jet flavor, performed with simulated samples, to account for the flavor dependence of the misidentification rate. The contribution of genuine τ_h candidates in the sideband regions selected with the relaxed identification requirement is taken into account when determining the background prediction, as described in [38].

5.2 Estimation of backgrounds with two genuine τ_h decays

The background contribution with two genuine τ_h decays originates mainly from the $Z/\gamma^* \to \tau\tau$+jets process, with smaller contributions originating from diboson production or processes with top quarks. We estimate this background using an embedding method [41] in which the reconstructed muons in a selected data sample of dimuon events are replaced by simulated τ leptons with the same kinematic properties as the original muons. This generates a set of hybrid events that rely on simulation only for the τ lepton decays. Consequently, they provide a better description of the underlying event, pileup, additional jets, detector noise and resolution effects compared to pure simulation samples. Since the embedded samples rely on the data for the description of these effects, no additional corrections for the pileup profile, jet energy scale, or b tagging efficiency are needed. Correction factors are applied to account for the efficiencies of the dimuon triggers and muon identification and isolation criteria used to select events. As the τ lepton decays are simulated, we apply scale factors to match the τ_h identification efficiency and energy scale in data. Correction factors are also applied to match the efficiencies of triggers used to select events for the search in data. Since the tracking efficiency in embedded events is higher than in data, scale factors are applied to account for this discrepancy. In order to save processing time, the sample selected for the detector simulation of τ lepton decays is restricted to events that will subsequently satisfy the selection criteria applied in analyses. This is done by applying a kinematic filter on the p_T and $|\eta|$ of the visible τ lepton decay products. Event weights are applied to account for the bias arising from the filter requirements. These corrections are described in more detail in [41].

We use a set of embedded samples in which both τ leptons are required to decay hadronically. We use an opposite-charge di-τ_h region in data to derive residual scale factors for the normalization of the embedded samples after all other correction factors are applied. These scale factors are designed to measure any remaining differences in the τ_h identification and trigger efficiencies between data and the embedded samples in a region that is kinematically similar to the SRs. This region consists of events passing the baseline selection, with the following additional requirements imposed on the mass and p_T of the di-τ_h system to improve the purity of genuine τ_h decays and enhance the contribution from $Z/\gamma^* \to \tau\tau$+jets: $50 < m_{\tau_h\tau_h} < 90\,\text{GeV}$ and $p_T^{\tau_h\tau_h} > 50\,\text{GeV}$. In order to ensure there is no overlap with the SRs and to suppress signal

contamination, we require that events in this region have $m_{T2} < 25\,\text{GeV}$ or $\Sigma m_T < 200\,\text{GeV}$. After subtracting the estimated contributions from misidentified τ_h events in this sample, we measure scale factors of 1.24 ± 0.03, 1.21 ± 0.03, and 1.16 ± 0.02 for 2016, 2017, and 2018 data, respectively, for the embedded events, with the uncertainties listed being statistical. We apply these scale factors, along with a conservative uncertainty corresponding to the full size of their deviations from unity, to the normalization of the embedded sample.

The genuine τ_h background prediction from the embedded sample accounts for SM events originating from processes in which the branching fractions for $\tau\tau$ and dimuon decays are identical, i.e., $Z/\gamma^* \to \tau\tau$+jets, $t\bar{t}$ (with or without extra vector bosons), single top quark, and diboson processes. Small contributions from top quark events in which the W boson from the top quark decay does not decay directly into a muon and a neutrino, e.g., from $W \to \tau\nu_\tau$, may be included in the sample selected to undergo the embedding process, resulting in a possible overestimation of the fraction of top quark events. In order to account for this effect, we check the normalization of top quark events estimated from the embedded sample in a control region selected by requiring at least one b-tagged jet, $m_{\tau_h\tau_h} > 100\,\text{GeV}$, and $p_T^{\text{miss}} > 50\,\text{GeV}$ to enrich the proportion of top quark events. Based on the level of agreement observed between data and the prediction from the embedded sample in this region, we assign an uncertainty of 10% in the expected fraction of top quark events in the embedded sample.

The embedded sample does not account for contributions from SM Higgs boson (H) events, for which the $\tau\tau$ and dimuon branching fractions are very different. We therefore include the estimated contribution from SM $H \to \tau\tau$ events from simulation in the total estimate of the genuine τ_h background. We find that the background contribution from SM $H \to \tau\tau$ events is small compared to the other backgrounds.

6 Systematic uncertainties

The dominant uncertainties in the background estimates are the statistical uncertainty driven by the limited event counts in the data sidebands or embedded samples used to obtain the estimates, and the systematic uncertainty (30%) assigned to the estimate of the τ_h misidentification rate that accounts for its dependence on jet flavor.

Because we use embedded events to estimate the background with two genuine τ_h decays, the prediction is less affected by systematic uncertainties than in the case of wholly simulated samples. For this background, we propagate uncertainties related to the trigger efficiency, τ_h identification efficiency, and τ_h energy scale. We also assign additional uncertainties as discussed in Section 5.2: a 10% uncertainty in the expected fraction of top quark events in the embedded samples estimated from simulation, and a normalization uncertainty determined by the full size of the deviations from unity of the normalization scale factors derived from the $Z/\gamma^* \to \tau\tau$+jets control region, weighted over the three years by the fractions of the integrated luminosity collected in each year. A 20% normalization uncertainty is assigned to the small contribution from SM $H \to \tau\tau$ events.

For the signal prediction obtained from simulation, we propagate uncertainties in the trigger efficiency, τ_h identification efficiency, τ_h energy scale, b tagging efficiency, pileup reweighting, jet energy scale and resolution, and unclustered energy. We also take into account the uncertainty in the integrated luminosity measurement. The integrated luminosities for the 2016, 2017, and 2018 data-taking years have 1.2–2.5% individual uncertainties [69–71], while the overall uncertainty for the 2016–2018 period is 1.6%. Uncertainties related to the renormalization and factorization scales, and to the modeling of ISR, are propagated to the signal prediction as well.

Table 2: Uncertainties in the analysis affecting signal and the SM backgrounds. The numbers indicate the percentage effect of propagating ± 1-standard deviation variations of the respective sources of uncertainty on the predicted signal and background yields, prior to a fit to the data. The ranges shown for signal refer to a representative benchmark model of $\widetilde{\tau}_{\mathrm{L}}$ pair production with $m(\widetilde{\tau}_{\mathrm{L}}) = 150\,\mathrm{GeV}$, $m(\widetilde{\chi}_1^0) = 1\,\mathrm{GeV}$.

	Uncertainty [%]		
Source	Genuine τ_{h}	Misidentified τ_{h}	Signal
Statistical	8.3–141	5.0–100	6.3–52
τ_{h} ID efficiency	7.2–7.8	—	6.2–6.4
τ_{h} ID vs. displacement	—	—	3.0
τ_{h} trigger efficiency	3.1–4.2	—	6.9–14
τ_{h} energy scale	0.1–35	—	1.6–44
τ_{h} misidentification rate	—	30–56	—
$p_{\mathrm{T}}^{\mathrm{miss}}$ trigger efficiency	1.0	—	1.5
Embedded normalization	19	—	—
Embedded top quark fraction	1.0–3.8	—	—
Jet energy scale	—	—	0.7–32
Jet energy resolution	—	—	1.3–55
Unclustered energy	—	—	0.5–32
b tagging	—	—	0.2–1.1
Pileup	—	—	1.0–28
Integrated luminosity	—	—	1.6
ISR	—	—	0.1–16
Renormalization/factorization scales	—	—	0.4–3.6

Since the τ_{h} identification and trigger efficiency correction factors applied to simulation, which are obtained from samples of $\mathrm{Z}/\gamma^* \to \tau\tau$+jets events with promptly produced τ leptons, do not account for the dependence of the τ_{h} candidate selection on the displacement of the decay position, we assign an additional uncertainty for this effect in signal events. The uncertainty is assessed via a comparison of τ_{h} impact parameter distributions between data and simulation in a control region that is mainly populated by $\mathrm{Z}/\gamma^* \to \tau\tau$+jets events, and the expected displacement of signal events for different $\widetilde{\tau}$ lifetimes. In order to probe the tails of the τ_{h} impact parameter distributions, which we expect to be populated by signal events with significant displacement, the data-to-simulation ratios observed in the control region at lower values of d_{xy} significance and IP3D are extrapolated to higher values via a linear fit when deriving this uncertainty. The size of the uncertainty ranges from 3% for promptly decaying $\widetilde{\tau}$, to 45% for $\widetilde{\tau}$ with $c\tau_0 = 2.5\,\mathrm{mm}$.

We treat statistical uncertainties as uncorrelated, while systematic uncertainties related to the same modeling effect are taken to be correlated across processes and data-taking periods. Table 2 lists the ranges of the uncertainty in the predicted yields for background and a benchmark signal model of $\widetilde{\tau}_{\mathrm{L}}$ pair production with $m(\widetilde{\tau}_{\mathrm{L}}) = 150\,\mathrm{GeV}$, $m(\widetilde{\chi}_1^0) = 1\,\mathrm{GeV}$ across all SRs corresponding to different sources.

7 Results and interpretation

Observed and predicted event yields for each SR are shown in Fig. 3 (upper) and summarized in Table 3 for the combined 2016–2018 data set. Figure 3 (lower) shows the background predictions after a maximum likelihood fit to the data under the background-only hypothe-

sis. The likelihood function is constructed from the observed and predicted event yields in all 31 SRs, with the uncertainties in the predicted yields incorporated as nuisance parameters in the fit. The normalization uncertainties affecting background and signal predictions are generally assumed to be log-normally distributed. For statistical uncertainties limited by small event counts in the embedded or simulation samples, or in the sideband regions in the data used to estimate the misidentified τ_h background, we use a Poisson distribution. The nuisance parameters are allowed to vary within their uncertainties in the fit. The uncertainties in the background predictions are reduced after the fit to the data. In general, the data are consistent with the prediction for the SM background. The most significant discrepancies between the data and the predicted background occur in SR bins 10 and 17, where we observe a deficit at approximately the 2-standard deviation level with respect to the pre-fit predictions, while a smaller deficit, at about the 1.2-standard deviation level, is observed in SR bin 18. Signal predictions are also shown in Fig. 3 (upper) for three benchmark models of left-handed prompt $\widetilde{\tau}$ pair production with $\widetilde{\tau}$ masses of 100, 150, and 200 GeV for an LSP mass of 1 GeV, and for one of long-lived $\widetilde{\tau}$ pair production in the maximally mixed scenario with a $\widetilde{\tau}$ mass of 150 GeV, an LSP mass of 1 GeV, and $c\tau_0(\widetilde{\tau}) = 0.5\,\text{mm}$.

We use the results to set upper limits on the cross section for the production of $\widetilde{\tau}$ pairs in the context of simplified models [26–28, 72] using all of the 31 exclusive SRs in a full statistical combination. The 95% CL upper limits on SUSY production cross sections are calculated using a modified frequentist approach with the CL_s criterion [73–75]. An asymptotic approximation is used for the test statistic [76].

Expected and observed 95% CL cross section upper limits as a function of the $\widetilde{\tau}$ mass for 4 choices of LSP mass are shown in Fig. 4 for $\widetilde{\tau}$ pair production with promptly decaying τ sleptons in the degenerate scenario, in which we assume that both left- and right-handed τ sleptons are produced with the same mass, and in Figs. 5 and 6, in the purely left- and right-handed scenarios, respectively. Also shown is the theoretical prediction for the cross section of $\widetilde{\tau}$ pair production in each scenario, as a function of the $\widetilde{\tau}$ mass. In general, the cross section limits become less stringent for higher values of the $\widetilde{\chi}_1^0$ mass as a result of smaller experimental acceptance, caused in particular by the decreasing probability of the τ_h candidate to exceed the 40 GeV $p_T^{\tau_h}$ threshold. Exclusion limits in the $\widetilde{\tau}$ vs $\widetilde{\chi}_1^0$ mass plane are presented in Fig. 7 for promptly decaying τ sleptons in the degenerate and purely left-handed scenarios. In the degenerate scenarios $\widetilde{\tau}$ masses up to 400 GeV are excluded at 95% CL under the hypothesis of a nearly massless LSP, while in the purely-left handed scenario, $\widetilde{\tau}$ masses between 115 and 340 GeV are excluded under the same hypothesis. For values of the $\widetilde{\tau}$ mass above $\approx$175–200 GeV, we generally observe exclusion limits that are approximately 1-standard deviation stronger than the expected exclusion limits, with the difference being largely driven by the deficits observed in SR bins 17 and 18. Exclusion limits for the purely right-handed scenario are not shown, because our sensitivity in this scenario is not yet sufficient to exclude a sizeable region in the $\widetilde{\tau}$ vs $\widetilde{\chi}_1^0$ mass plane.

Expected and observed 95% CL cross section upper limits are shown in Fig. 8 for long-lived τ sleptons in the maximally mixed scenario, under the hypothesis of a nearly massless LSP. For a $\widetilde{\tau}$ lifetime corresponding to $c\tau_0 = 0.1\,\text{mm}$, $\widetilde{\tau}$ masses between 150 and 220 GeV are excluded in this scenario, with the mass limits being assessed from the intersection of the observed exclusion curve with the theoretical prediction. The search sensitivity is reduced for longer $\widetilde{\tau}$ lifetimes because the DEEPTAU algorithm is currently optimized for promptly produced τ_h candidates and is less efficient for more significantly displaced τ_h candidates.

Table 3: Predicted SM background yields, observed event counts, and predicted signal yields for two benchmark models with a $\widetilde{\tau}$ mass of 150 GeV and an LSP mass of 1 GeV, in all prompt and displaced SRs as labeled in Table 1. For the prompt signal model shown, we assume left-handed $\widetilde{\tau}$ pair production, while for the displaced signal model we assume a maximally mixed scenario and $c\tau_0(\widetilde{\tau}) = 0.5\,\text{mm}$. The uncertainties listed are the sum in quadrature of the statistical and systematic components. For any estimate with no events in the data sideband, embedded, or simulation sample corresponding to a given SR selection, we provide the one standard deviation upper bound evaluated for that estimate.

SR bin	Genuine τ_h	Misidentified τ_h	Total SM	Observed	Prompt signal	Displaced τ_h signal
1	18.8 ± 4.4	39.6 ± 8.5	58.4 ± 9.6	65	0.6 ± 0.1	0.1 ± 0.1
2	25.9 ± 6.2	21.8 ± 5.5	47.7 ± 8.2	40	1.7 ± 0.3	0.6 ± 0.2
3	21.4 ± 4.9	26.1 ± 6.0	47.5 ± 7.7	38	1.4 ± 0.3	0.3 ± 0.1
4	$1.3^{+1.0}_{-0.6}$	$2.1^{+1.5}_{-1.4}$	$3.4^{+1.8}_{-1.5}$	4	0.5 ± 0.1	0.1 ± 0.1
5	$0.5^{+0.5}_{-0.3}$	$0.1^{+0.7}_{-0.1}$	$0.6^{+0.9}_{-0.4}$	1	0.0 ± 0.0	<0.6
6	$1.0^{+0.9}_{-0.6}$	$1.6^{+1.1}_{-0.9}$	$2.5^{+1.5}_{-1.1}$	1	0.0 ± 0.0	<0.6
7	14.6 ± 3.9	3.7 ± 3.0	18.3 ± 4.9	28	1.8 ± 0.3	0.4 ± 0.2
8	$2.5^{+1.1}_{-0.9}$	2.7 ± 1.5	$5.2^{+1.9}_{-1.8}$	7	0.6 ± 0.1	0.1 ± 0.0
9	$2.1^{+1.3}_{-1.0}$	2.2 ± 1.6	$4.3^{+2.1}_{-1.9}$	4	1.9 ± 0.3	0.4 ± 0.1
10	$1.8^{+0.9}_{-0.7}$	$2.7^{+1.3}_{-1.1}$	$4.5^{+1.6}_{-1.3}$	0	0.8 ± 0.2	0.1 ± 0.1
11	$5.2^{+2.1}_{-1.8}$	4.2 ± 2.2	$9.4^{+3.1}_{-2.9}$	7	1.2 ± 0.2	0.3 ± 0.1
12	$1.5^{+1.3}_{-0.9}$	$1.7^{+1.4}_{-1.2}$	$3.2^{+1.9}_{-1.5}$	3	1.4 ± 0.3	0.4 ± 0.1
13	$1.1^{+1.1}_{-0.6}$	$0.1^{+1.0}_{-0.1}$	$1.1^{+1.5}_{-0.6}$	3	1.3 ± 0.2	0.3 ± 0.1
14	$0.2^{+0.5}_{-0.2}$	$0.5^{+0.8}_{-0.4}$	$0.7^{+0.9}_{-0.5}$	0	0.2 ± 0.1	0.0 ± 0.0
15	$8.9^{+2.9}_{-2.6}$	2.2 ± 2.6	$11.1^{+3.9}_{-3.7}$	17	3.0 ± 0.4	0.6 ± 0.2
16	$3.2^{+1.6}_{-1.3}$	<1.0	$3.2^{+1.9}_{-1.3}$	4	3.1 ± 0.5	0.7 ± 0.2
17	$2.5^{+1.4}_{-1.1}$	$3.0^{+1.5}_{-1.3}$	$5.5^{+2.1}_{-1.7}$	0	2.3 ± 0.4	0.6 ± 0.2
18	$0.7^{+1.0}_{-0.5}$	$0.9^{+0.8}_{-0.5}$	$1.6^{+1.3}_{-0.7}$	0	1.9 ± 0.3	0.4 ± 0.1
19	34.6 ± 7.9	23.8 ± 5.5	58.4 ± 9.6	45	0.9 ± 0.2	0.3 ± 0.1
20	35.7 ± 7.7	17.7 ± 4.8	53.4 ± 9.0	53	0.6 ± 0.1	0.3 ± 0.1
21	19.5 ± 4.9	5.4 ± 2.6	24.9 ± 5.5	15	0.7 ± 0.2	0.2 ± 0.1
22	11.4 ± 3.0	8.0 ± 3.0	19.4 ± 4.2	15	0.9 ± 0.2	0.2 ± 0.1
23	$4.5^{+1.5}_{-1.3}$	2.3 ± 1.6	$6.8^{+2.2}_{-2.1}$	6	0.3 ± 0.1	0.0 ± 0.0
24	$7.3^{+2.7}_{-2.4}$	4.7 ± 2.4	$12.0^{+3.6}_{-3.4}$	10	0.5 ± 0.1	0.2 ± 0.1
25	$4.6^{+1.9}_{-1.6}$	$2.3^{+1.4}_{-1.2}$	$6.9^{+2.3}_{-2.0}$	2	0.6 ± 0.1	0.1 ± 0.1
26	$2.3^{+1.3}_{-1.0}$	<1.3	$2.3^{+1.9}_{-1.0}$	3	0.4 ± 0.1	0.2 ± 0.1
27	15.8 ± 4.1	2.8 ± 3.1	18.6 ± 5.2	23	2.8 ± 0.4	0.8 ± 0.2
28	$0.9^{+0.9}_{-0.5}$	$1.4^{+1.1}_{-0.9}$	$2.3^{+1.5}_{-1.0}$	2	1.0 ± 0.2	0.4 ± 0.1
29	$1.5^{+1.2}_{-0.8}$	$1.9^{+1.4}_{-1.1}$	$3.4^{+1.9}_{-1.4}$	3	0.6 ± 0.1	0.1 ± 0.1
30	$3.6^{+1.5}_{-1.3}$	$0.7^{+1.3}_{-0.7}$	$4.3^{+2.0}_{-1.5}$	5	0.9 ± 0.2	2.6 ± 0.7
31	<0.5	<0.4	$0.0^{+0.7}_{-0.0}$	0	0.2 ± 0.1	1.0 ± 0.3

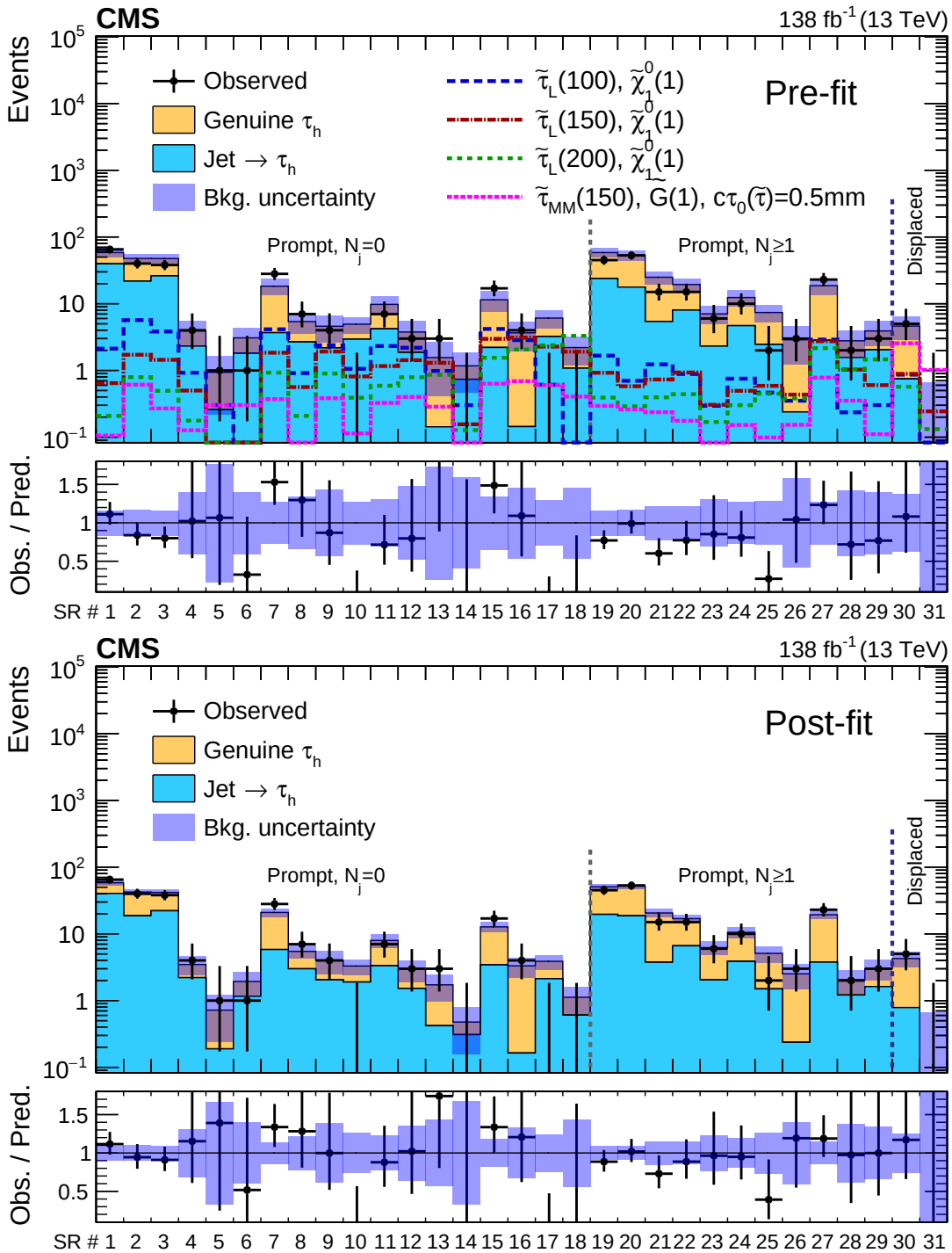

Figure 3: Event counts and predicted yields in each SR for the SM background before (upper) and after (lower) a maximum likelihood fit to the data under the background-only hypothesis. The yields expected for 3 benchmark models of left-handed $\tilde{\tau}$ pair production assuming prompt $\tilde{\tau}$ decays, and one model of long-lived $\tilde{\tau}$ pair production in the maximally mixed scenario ($\tilde{\tau}_{\mathrm{MM}}$) are overlaid in the pre-fit case. The numbers in parentheses correspond to the masses of the $\tilde{\tau}$ and LSP in units of GeV for the different signal models. The lower panels show the ratio of the observed event counts to the total SM background prediction. The first 29 bins correspond to the prompt SRs, while bins 30 and 31 correspond to the displaced SRs, as labeled in Table 1.

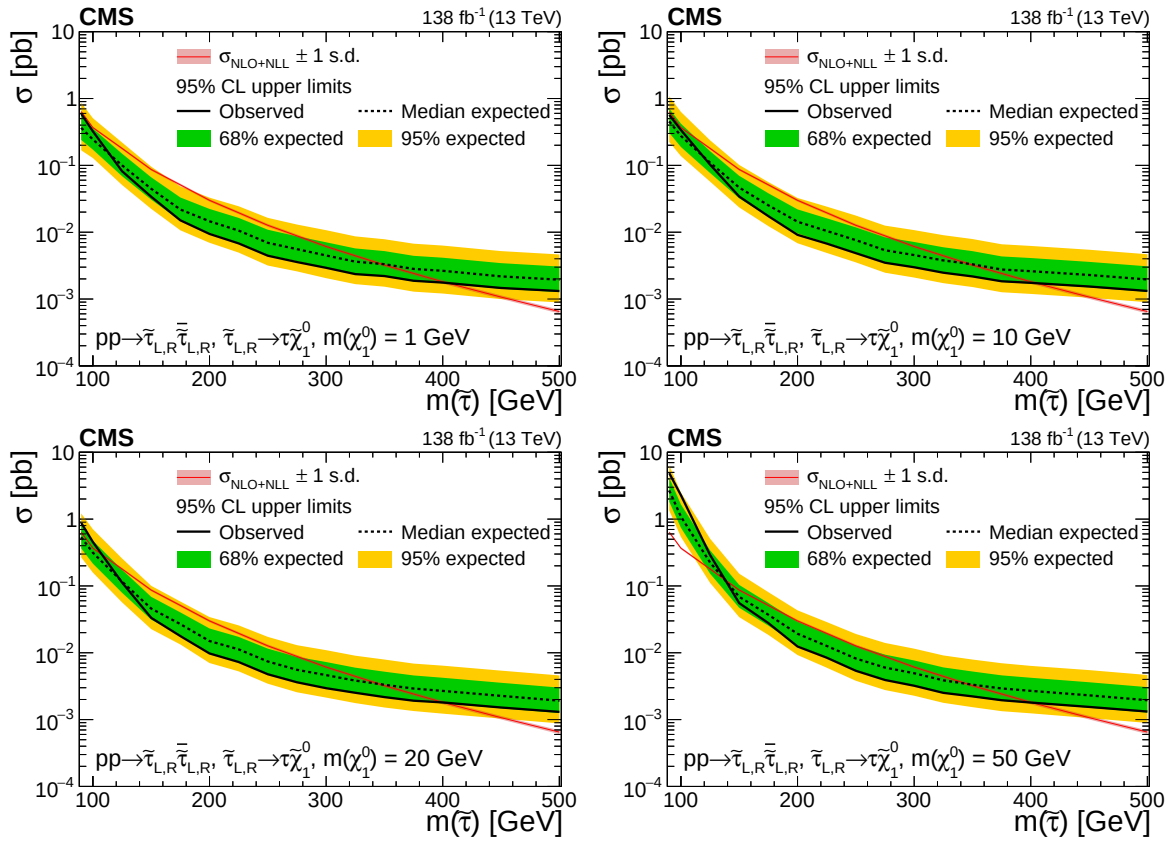

Figure 4: Expected and observed 95% CL cross section upper limits as functions of the $\widetilde{\tau}$ mass in the degenerate $\widetilde{\tau}$ scenario for $\widetilde{\chi}_1^0$ masses of 1, 10, 20, and 50 GeV (upper left to lower right). The inner (green) band and the outer (yellow) band indicate the regions containing 68 and 95%, respectively, of the distribution of limits expected under the background-only hypothesis. The red line and thin shaded band indicate the NLO+NLL prediction for the signal production cross section calculated with RESUMMINO [29], and its uncertainty.

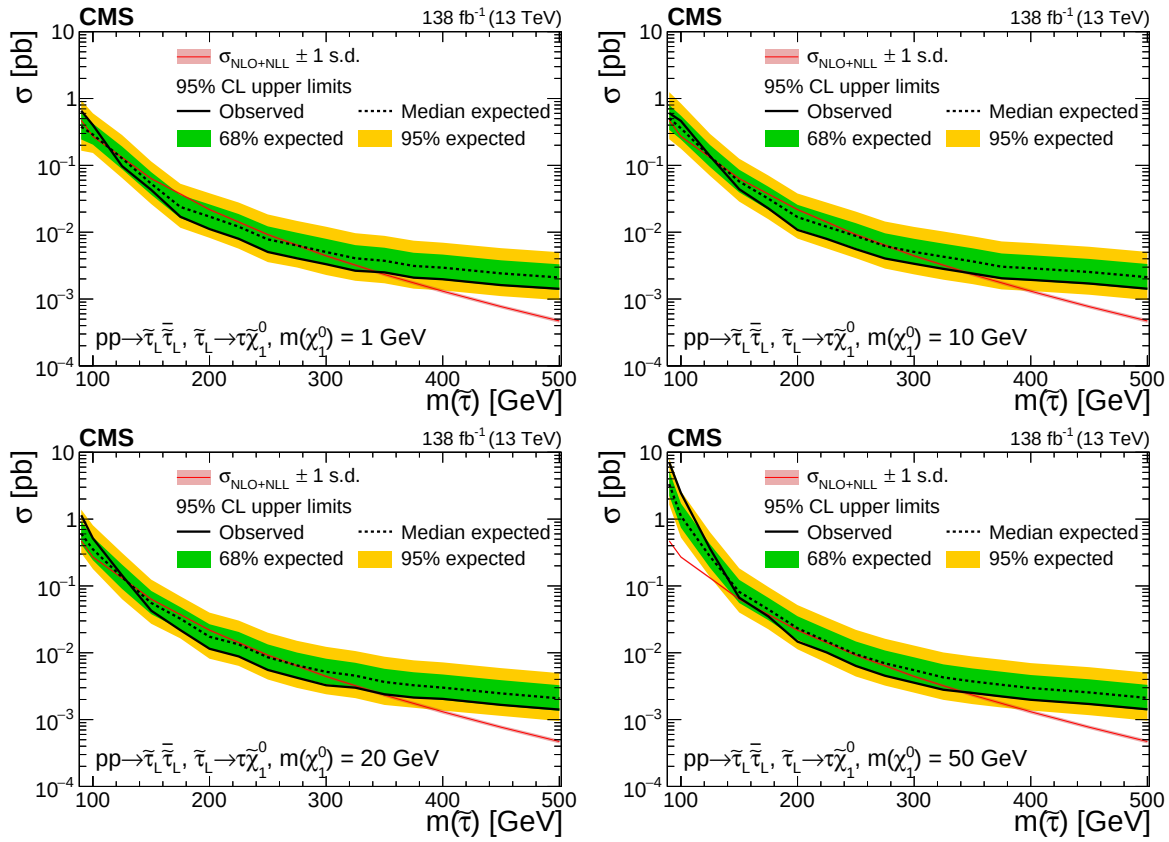

Figure 5: Expected and observed 95% CL cross section upper limits as functions of the $\tilde{\tau}$ mass in the purely left-handed $\tilde{\tau}$ scenario for $\tilde{\chi}_1^0$ masses of 1, 10, 20, and 50 GeV (upper left to lower right). The inner (green) band and the outer (yellow) band indicate the regions containing 68 and 95%, respectively, of the distribution of limits expected under the background-only hypothesis. The red line and thin shaded band indicate the NLO+NLL prediction for the signal production cross section calculated with RESUMMINO [29], and its uncertainty.

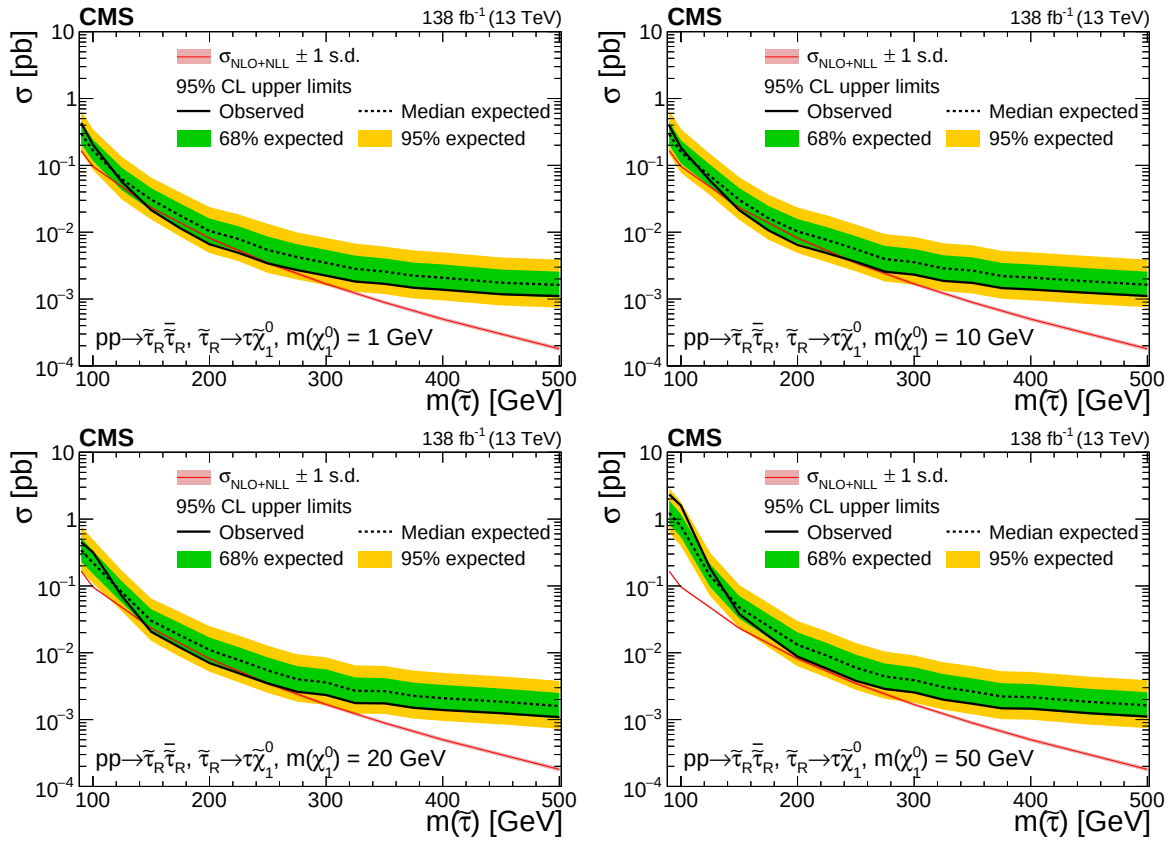

Figure 6: Expected and observed 95% CL cross section upper limits as functions of the $\tilde{\tau}$ mass in the purely right-handed $\tilde{\tau}$ scenario for $\tilde{\chi}_1^0$ masses of 1, 10, 20, and 50 GeV (upper left to lower right). The inner (green) band and the outer (yellow) band indicate the regions containing 68 and 95%, respectively, of the distribution of limits expected under the background-only hypothesis. The red line and thin shaded band indicate the NLO+NLL prediction for the signal production cross section calculated with RESUMMINO [29], and its uncertainty.

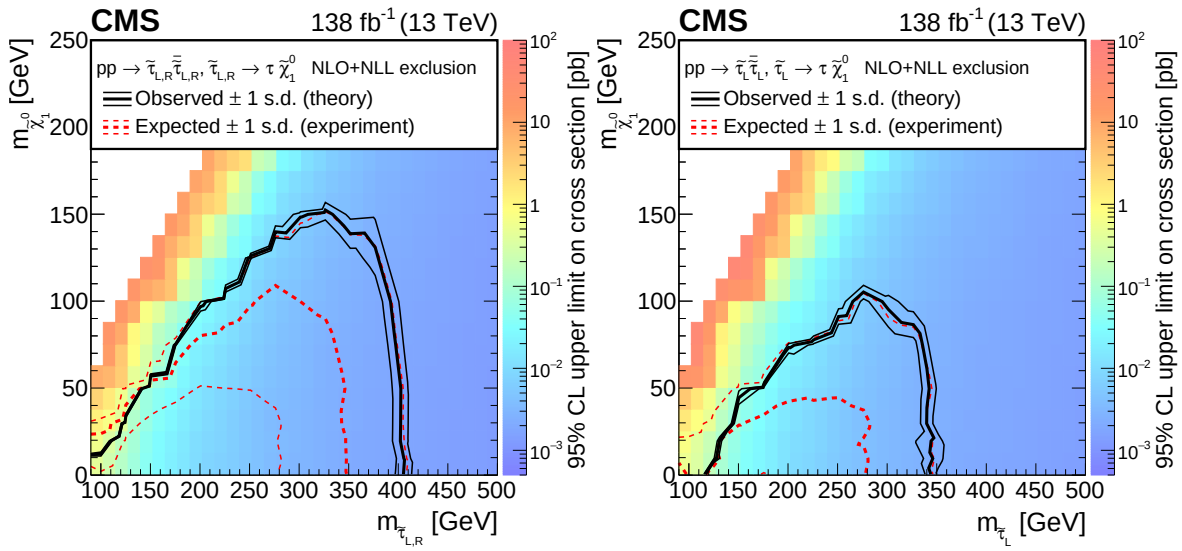

Figure 7: Upper limits at 95% CL on the cross section for degenerate (left) and purely left-handed (right) $\widetilde{\tau}$ pair production in the $m(\widetilde{\tau})$-$m(\widetilde{\chi}_1^0)$ plane. The thick black (red) curves show the observed (expected) exclusion limits assuming NLO+NLL predictions for the signal cross sections. The thin black curves represent the variations in the observed limits obtained when these cross sections are varied by their ± 1 standard deviation uncertainties. The thin dashed red curves indicate the region containing 68% of the distribution of limits expected under the background-only hypothesis.

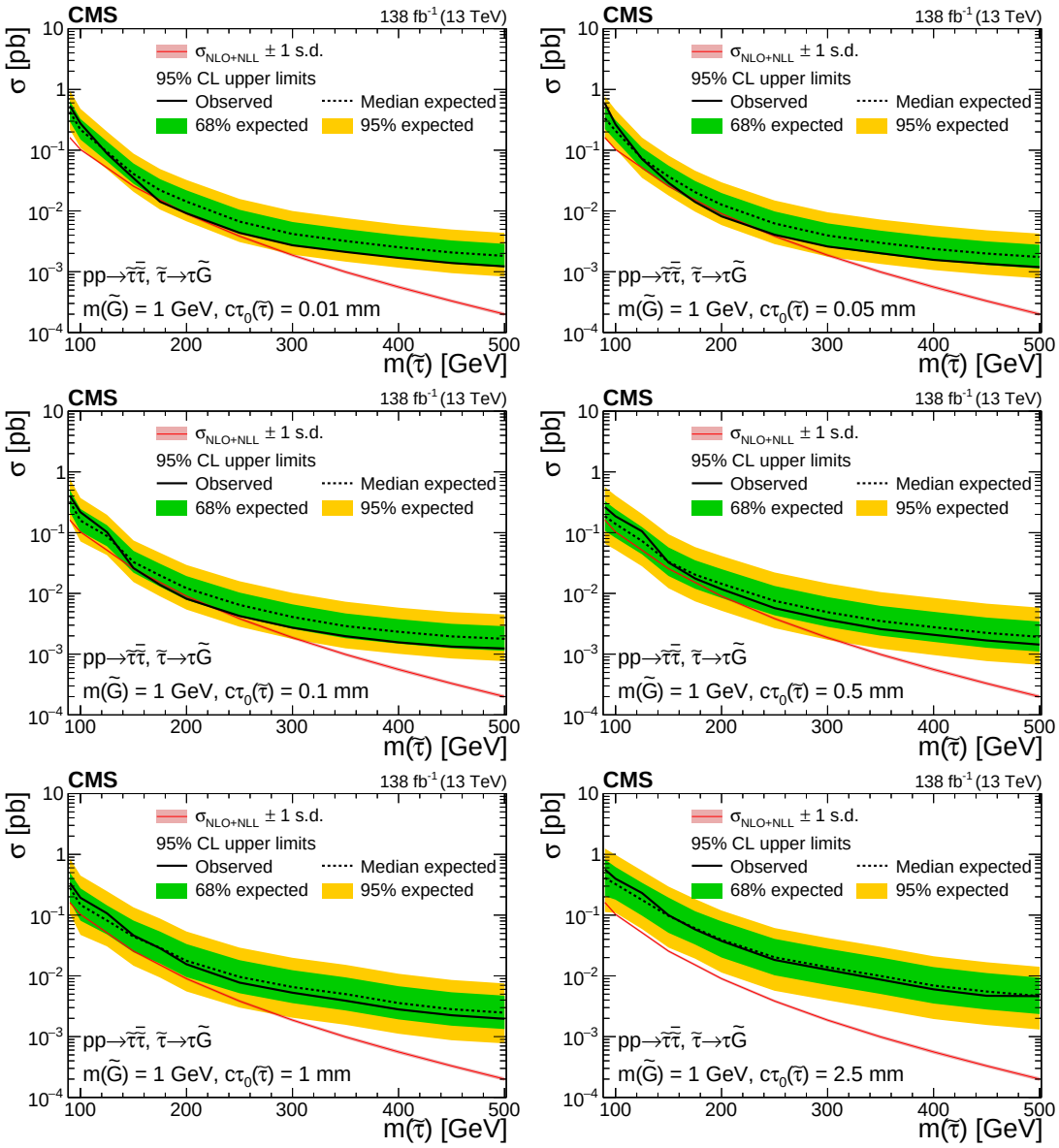

Figure 8: Expected and observed 95% CL cross section upper limits as functions of the $\tilde{\tau}$ mass for long-lived $\tilde{\tau}$ in the maximally mixed scenario for an LSP mass of 1 GeV, and for $c\tau_0$ values of 0.01, 0.05, 0.1, 0.5, 1, and 2.5 mm (upper left to lower right). The inner (green) band and the outer (yellow) band indicate the regions containing 68 and 95%, respectively, of the distribution of limits expected under the background-only hypothesis. The red line and thin shaded band indicate the NLO+NLL prediction for the signal production cross section calculated with RESUMMINO [29], and its uncertainty.

8 Summary

A search for direct τ slepton ($\widetilde{\tau}$) pair production has been performed in proton-proton collisions at a center-of-mass energy of 13 TeV in events with two hadronically decaying τ leptons and significant missing transverse momentum. The data used for this search correspond to an integrated luminosity of 138 fb^{-1} collected in 2016–2018 with the CMS detector. Both prompt and displaced decays of the τ slepton are studied. Thirty-one different search regions are used in the analysis, based on kinematic observables that exploit expected differences between signal and background. No significant excess of events above the expected standard model background has been observed. Upper limits have been set on the cross section for direct $\widetilde{\tau}$ pair production for simplified models in which each $\widetilde{\tau}$ decays to a τ lepton and the lightest supersymmetric particle (LSP). For purely left-handed $\widetilde{\tau}$ pair production with prompt decays, $\widetilde{\tau}$ masses between 115 and 340 GeV are excluded at 95% confidence level for the case of a nearly massless LSP, while for the degenerate production of left- and right-handed $\widetilde{\tau}$ pairs, $\widetilde{\tau}$ masses up to 400 GeV are excluded under the same hypothesis. The limits observed are the most stringent obtained thus far in the case of direct $\widetilde{\tau}$ pair production with prompt $\widetilde{\tau}$ decays, for both the purely left-handed and degenerate production scenarios. They represent a considerable improvement in sensitivity with respect to the previous CMS search reported in Ref. [38]. In the context of long-lived τ sleptons, final states with displaced τ_{h} candidates are investigated for the first time. In a scenario with $c\tau_0(\widetilde{\tau}) = 0.1$ mm, where τ_0 denotes the mean proper lifetime of the $\widetilde{\tau}$, masses between 150 and 220 GeV are excluded for the case that the LSP is nearly massless.

References

[1] P. Ramond, "Dual theory for free fermions", *Phys. Rev. D* **3** (1971) 2415, doi:10.1103/PhysRevD.3.2415.

[2] Y. A. Gol'fand and E. P. Likhtman, "Extension of the algebra of Poincaré group generators and violation of P invariance", *JETP Lett.* **13** (1971) 323.

[3] A. Neveu and J. H. Schwarz, "Factorizable dual model of pions", *Nucl. Phys. B* **31** (1971) 86, doi:10.1016/0550-3213(71)90448-2.

[4] D. V. Volkov and V. P. Akulov, "Possible universal neutrino interaction", *JETP Lett.* **16** (1972) 438.

[5] J. Wess and B. Zumino, "A Lagrangian model invariant under supergauge transformations", *Phys. Lett. B* **49** (1974) 52, doi:10.1016/0370-2693(74)90578-4.

[6] J. Wess and B. Zumino, "Supergauge transformations in four dimensions", *Nucl. Phys. B* **70** (1974) 39, doi:10.1016/0550-3213(74)90355-1.

[7] P. Fayet, "Supergauge invariant extension of the Higgs mechanism and a model for the electron and its neutrino", *Nucl. Phys. B* **90** (1975) 104, doi:10.1016/0550-3213(75)90636-7.

[8] H. P. Nilles, "Supersymmetry, supergravity and particle physics", *Phys. Rep.* **110** (1984) 1, doi:10.1016/0370-1573(84)90008-5.

[9] E. Gildener, "Gauge symmetry hierarchies", *Phys. Rev. D* **14** (1976) 1667, doi:10.1103/PhysRevD.14.1667.

[10] M. J. G. Veltman, "Second threshold in weak interactions", *Acta Phys. Polon. B* **8** (1977) 475.

[11] G. 't Hooft, "Naturalness, chiral symmetry, and spontaneous chiral symmetry breaking", *NATO Sci. Ser. B* **59** (1980) 135.

[12] E. Witten, "Dynamical breaking of supersymmetry", *Nucl. Phys. B* **188** (1981) 513, doi:10.1016/0550-3213(81)90006-7.

[13] G. R. Farrar and P. Fayet, "Phenomenology of the production, decay, and detection of new hadronic states associated with supersymmetry", *Phys. Lett. B* **76** (1978) 575, doi:10.1016/0370-2693(78)90858-4.

[14] H. Goldberg, "Constraint on the photino mass from cosmology", *Phys. Rev. Lett.* **50** (1983) 1419, doi:10.1103/PhysRevLett.50.1419. [Erratum: doi:10.1103/PhysRevLett.103.099905].

[15] J. R. Ellis et al., "Supersymmetric relics from the Big Bang", *Nucl. Phys. B* **238** (1984) 453, doi:10.1016/0550-3213(84)90461-9.

[16] G. Jungman, M. Kamionkowski, and K. Griest, "Supersymmetric dark matter", *Phys. Rept.* **267** (1996) 195, doi:10.1016/0370-1573(95)00058-5, arXiv:hep-ph/9506380.

[17] G. Hinshaw et al., "Nine-year Wilkinson Microwave Anisotropy Probe (WMAP) observations: cosmological parameter results", *Astrophys. J. Suppl.* **208** (2013) 19, doi:10.1088/0067-0049/208/2/19, arXiv:1212.5226.

[18] K. Griest and D. Seckel, "Three exceptions in the calculation of relic abundances", *Phys. Rev. D* **43** (1991) 3191, doi:10.1103/PhysRevD.43.3191.

[19] D. A. Vasquez, G. Bélanger, and C. Boehm, "Revisiting light neutralino scenarios in the MSSM", *Phys. Rev. D* **84** (2011) 095015, doi:10.1103/PhysRevD.84.095015, arXiv:1108.1338.

[20] S. F. King, J. P. Roberts, and D. P. Roy, "Natural dark matter in SUSY GUTs with non-universal gaugino masses", *JHEP* **10** (2007) 106, doi:10.1088/1126-6708/2007/10/106, arXiv:0705.4219.

[21] M. Battaglia et al., "Proposed post-LEP benchmarks for supersymmetry", *Eur. Phys. J. C* **22** (2001) 535, doi:10.1007/s100520100792, arXiv:hep-ph/0106204.

[22] R. L. Arnowitt et al., "Determining the dark matter relic density in the minimal supergravity stau-neutralino coannihilation region at the Large Hadron Collider", *Phys. Rev. Lett.* **100** (2008) 231802, doi:10.1103/PhysRevLett.100.231802, arXiv:0802.2968.

[23] G. Bélanger, S. Biswas, C. Boehm, and B. Mukhopadhyaya, "Light neutralino dark matter in the MSSM and its implication for LHC searches for staus", *JHEP* **12** (2012) 076, doi:10.1007/JHEP12(2012)076, arXiv:1206.5404.

[24] E. Arganda, V. Martin-Lozano, A. D. Medina, and N. Mileo, "Potential discovery of staus through heavy Higgs boson decays at the LHC", *JHEP* **09** (2018) 056, doi:10.1007/JHEP09(2018)056, arXiv:1804.10698.

[25] J. A. Evans and J. Shelton, "Long-lived staus and displaced leptons at the LHC", *JHEP* **04** (2016) 056, doi:10.1007/JHEP04(2016)056, arXiv:1601.01326.

[26] J. Alwall, P. Schuster, and N. Toro, "Simplified models for a first characterization of new physics at the LHC", *Phys. Rev. D* **79** (2009) 075020, doi:10.1103/PhysRevD.79.075020, arXiv:0810.3921.

[27] J. Alwall, M.-P. Le, M. Lisanti, and J. Wacker, "Model-independent jets plus missing energy searches", *Phys. Rev. D* **79** (2009) 015005, doi:10.1103/PhysRevD.79.015005, arXiv:0809.3264.

[28] LHC New Physics Working Group, "Simplified models for LHC new physics searches", *J. Phys. G* **39** (2012) 105005, doi:10.1088/0954-3899/39/10/105005, arXiv:1105.2838.

[29] B. Fuks, M. Klasen, D. R. Lamprea, and M. Rothering, "Revisiting slepton pair production at the Large Hadron Collider", *JHEP* **01** (2014) 168, doi:10.1007/JHEP01(2014)168, arXiv:1310.2621.

[30] ALEPH Collaboration, "Search for scalar leptons in e^+e^- collisions at center-of-mass energies up to 209 GeV", *Phys. Lett. B* **526** (2002) 206, doi:10.1016/S0370-2693(01)01494-0, arXiv:hep-ex/0112011.

[31] DELPHI Collaboration, "Searches for supersymmetric particles in e^+e^- collisions up to 208 GeV and interpretation of the results within the MSSM", *Eur. Phys. J. C* **31** (2003) 421, doi:10.1140/epjc/s2003-01355-5, arXiv:hep-ex/0311019.

[32] L3 Collaboration, "Search for scalar leptons and scalar quarks at LEP", *Phys. Lett. B* **580** (2004) 37, doi:10.1016/j.physletb.2003.10.010, arXiv:hep-ex/0310007.

[33] OPAL Collaboration, "Search for anomalous production of dilepton events with missing transverse momentum in e^+e^- collisions at $\sqrt{s}$ = 183 GeV to 209 GeV", *Eur. Phys. J. C* **32** (2004) 453, doi:10.1140/epjc/s2003-01466-y, arXiv:hep-ex/0309014.

[34] ATLAS Collaboration, "Search for the direct production of charginos, neutralinos and staus in final states with at least two hadronically decaying taus and missing transverse momentum in pp collisions at $\sqrt{s}$ = 8 TeV with the ATLAS detector", *JHEP* **10** (2014) 96, doi:10.1007/JHEP10(2014)096, arXiv:1407.0350.

[35] ATLAS Collaboration, "Search for the electroweak production of supersymmetric particles in $\sqrt{s} = 8$ TeV pp collisions with the ATLAS detector", *Phys. Rev. D* **93** (2016) 052002, doi:10.1103/PhysRevD.93.052002, arXiv:1509.07152.

[36] CMS Collaboration, "Search for electroweak production of charginos in final states with two tau leptons in pp collisions at $\sqrt{s} = 8$ TeV", *JHEP* **04** (2017) 018, doi:10.1007/JHEP04(2017)018, arXiv:1610.04870.

[37] ATLAS Collaboration, "Search for direct stau production in events with two hadronic τ-leptons in $\sqrt{s} = 13$ TeV pp collisions with the ATLAS detector", *Phys. Rev. D* **101** (2020) 032009, doi:10.1103/PhysRevD.101.032009, arXiv:1911.06660.

[38] CMS Collaboration, "Search for direct pair production of supersymmetric partners to the τ lepton in proton-proton collisions at $\sqrt{s} = 13$ TeV", *Eur. Phys. J. C* **80** (2020) 189, doi:10.1140/epjc/s10052-020-7739-7, arXiv:1907.13179.

[39] OPAL Collaboration, "Searches for gauge-mediated supersymmetry breaking topologies in e^+e^- collisions at LEP2", *Eur. Phys. J. C* **46** (2006) 307, doi:10.1140/epjc/s2006-02524-8, arXiv:hep-ex/0507048.

[40] ATLAS Collaboration, "Search for displaced leptons in $\sqrt{s} = 13$ TeV pp collisions with the ATLAS detector", *Phys. Rev. Lett.* **127** (2021) 051802, doi:10.1103/PhysRevLett.127.051802, arXiv:2011.07812.

[41] CMS Collaboration, "An embedding technique to determine $\tau\tau$ backgrounds in proton-proton collision data", *JINST* **14** (2019) P06032, doi:10.1088/1748-0221/14/06/P06032, arXiv:1903.01216.

[42] CMS Collaboration, "Identification of hadronic tau lepton decays using a deep neural network", 2022. arXiv:2201.08458. Submitted to *JINST*.

[43] HEPData record for this analysis, 2022. doi:10.17182/hepdata.131308.

[44] CMS Collaboration, "Performance of the CMS Level-1 trigger in proton-proton collisions at $\sqrt{s} = 13$ TeV", *JINST* **15** (2020) P10017, doi:10.1088/1748-0221/15/10/P10017, arXiv:2006.10165.

[45] CMS Collaboration, "The CMS trigger system", *JINST* **12** (2017) P01020, doi:10.1088/1748-0221/12/01/P01020, arXiv:1609.02366.

[46] CMS Collaboration, "Particle-flow reconstruction and global event description with the CMS detector", *JINST* **12** (2017) P10003, doi:10.1088/1748-0221/12/10/P10003, arXiv:1706.04965.

[47] CMS Collaboration, "Performance of missing transverse momentum reconstruction in proton-proton collisions at $\sqrt{s} = 13$ TeV using the CMS detector", *JINST* **14** (2019) P07004, doi:10.1088/1748-0221/14/07/P07004, arXiv:1903.06078.

[48] CMS Collaboration, "Technical proposal for the Phase-II upgrade of the Compact Muon Solenoid", CMS Technical Proposal CERN-LHCC-2015-010, CMS-TDR-15-02, 2015.

[49] M. Cacciari, G. P. Salam, and G. Soyez, "The anti-k_T jet clustering algorithm", *JHEP* **04** (2008) 063, doi:10.1088/1126-6708/2008/04/063, arXiv:0802.1189.

[50] M. Cacciari, G. P. Salam, and G. Soyez, "FastJet user manual", *Eur. Phys. J. C* **72** (2012) 1896, doi:10.1140/epjc/s10052-012-1896-2, arXiv:1111.6097.

[51] CMS Collaboration, "Jet energy scale and resolution in the CMS experiment in pp collisions at 8 TeV", *JINST* **12** (2017) P02014, doi:10.1088/1748-0221/12/02/P02014, arXiv:1607.03663.

[52] CMS Collaboration, "Identification of heavy-flavour jets with the CMS detector in pp collisions at 13 TeV", *JINST* **13** (2018) P05011, doi:10.1088/1748-0221/13/05/P05011, arXiv:1712.07158.

[53] CMS Collaboration, "Performance of reconstruction and identification of τ leptons decaying to hadrons and ν_τ in pp collisions at $\sqrt{s} = 13$ TeV", *JINST* **13** (2018) P10005, doi:10.1088/1748-0221/13/10/P10005, arXiv:1809.02816.

[54] J. Alwall et al., "The automated computation of tree-level and next-to-leading order differential cross sections, and their matching to parton shower simulations", *JHEP* **07** (2014) 079, doi:10.1007/JHEP07(2014)079, arXiv:1405.0301.

[55] T. Sjöstrand et al., "An introduction to PYTHIA 8.2", *Comput. Phys. Commun.* **191** (2015) 159, doi:10.1016/j.cpc.2015.01.024, arXiv:1410.3012.

[56] CMS Collaboration, "Event generator tunes obtained from underlying event and multiparton scattering measurements", *Eur. Phys. J. C* **76** (2016) 155, doi:10.1140/epjc/s10052-016-3988-x, arXiv:1512.00815.

[57] CMS Collaboration, "Extraction and validation of a new set of CMS PYTHIA8 tunes from underlying-event measurements", *Eur. Phys. J. C* **80** (2020) 4, doi:10.1140/epjc/s10052-019-7499-4, arXiv:1903.12179.

[58] NNPDF Collaboration, "Parton distributions for the LHC Run II", *JHEP* **04** (2015) 040, doi:10.1007/JHEP04(2015)040, arXiv:1410.8849.

[59] GEANT4 Collaboration, "GEANT4 — a simulation toolkit", *Nucl. Instrum. Meth. A* **506** (2003) 250, doi:10.1016/S0168-9002(03)01368-8.

[60] A. Kalogeropoulos and J. Alwall, "The SysCalc code: A tool to derive theoretical systematic uncertainties", 2018. arXiv:1801.08401.

[61] P. Nason, "A new method for combining NLO QCD with shower Monte Carlo algorithms", *JHEP* **11** (2004) 040, doi:10.1088/1126-6708/2004/11/040, arXiv:hep-ph/0409146.

[62] S. Frixione, P. Nason, and C. Oleari, "Matching NLO QCD computations with parton shower simulations: the POWHEG method", *JHEP* **11** (2007) 070, doi:10.1088/1126-6708/2007/11/070, arXiv:0709.2092.

[63] S. Alioli, P. Nason, C. Oleari, and E. Re, "A general framework for implementing NLO calculations in shower Monte Carlo programs: the POWHEG BOX", *JHEP* **06** (2010) 043, doi:10.1007/JHEP06(2010)043, arXiv:1002.2581.

[64] E. Re, "Single-top Wt-channel production matched with parton showers using the POWHEG method", *Eur. Phys. J. C* **71** (2011) 1547, doi:10.1140/epjc/s10052-011-1547-z, arXiv:1009.2450.

[65] CMS Collaboration, "Search for top-squark pair production in the single-lepton final state in pp collisions at $\sqrt{s}$ = 8 TeV", *Eur. Phys. J. C* **73** (2013) 2677, doi:10.1140/epjc/s10052-013-2677-2, arXiv:1308.1586.

[66] C. G. Lester and D. J. Summers, "Measuring masses of semi-invisibly decaying particle pairs produced at hadron colliders", *Phys. Lett. B* **463** (1999) 99, doi:10.1016/S0370-2693(99)00945-4, arXiv:hep-ph/9906349.

[67] A. Barr, C. Lester, and P. Stephens, "m_{T2}: the truth behind the glamour", *J. Phys. G* **29** (2003) 2343, doi:10.1088/0954-3899/29/10/304, arXiv:hep-ph/0304226.

[68] C. G. Lester and B. Nachman, "Bisection-based asymmetric m_{T2} computation: a higher precision calculator than existing symmetric methods", *JHEP* **03** (2015) 100, doi:10.1007/JHEP03(2015)100, arXiv:1411.4312.

[69] CMS Collaboration, "Precision luminosity measurement in proton-proton collisions at $\sqrt{s} = 13$ TeV in 2015 and 2016 at CMS", *Eur. Phys. J. C* **81** (2021) 800, doi:10.1140/epjc/s10052-021-09538-2, arXiv:2104.01927.

[70] CMS Collaboration, "CMS luminosity measurement for the 2017 data-taking period at $\sqrt{s} = 13$ TeV", CMS Physics Analysis Summary CMS-PAS-LUM-17-004, 2018.

[71] CMS Collaboration, "CMS luminosity measurement for the 2018 data-taking period at $\sqrt{s} = 13$ TeV", CMS Physics Analysis Summary CMS-PAS-LUM-18-002, 2019.

[72] CMS Collaboration, "Interpretation of searches for supersymmetry with simplified models", *Phys. Rev. D* **88** (2013) 052017, doi:10.1103/PhysRevD.88.052017, arXiv:1301.2175.

[73] T. Junk, "Confidence level computation for combining searches with small statistics", *Nucl. Instrum. Meth. A* **434** (1999) 435, doi:10.1016/S0168-9002(99)00498-2, arXiv:hep-ex/9902006.

[74] A. L. Read, "Presentation of search results: the CL_s technique", *J. Phys. G* **28** (2002) 2693, doi:10.1088/0954-3899/28/10/313.

[75] ATLAS and CMS Collaborations, and the LHC Higgs Combination Group, "Procedure for the LHC Higgs boson search combination in Summer 2011", Technical Report CMS-NOTE-2011-005, ATL-PHYS-PUB-2011-11, 2011.

[76] G. Cowan, K. Cranmer, E. Gross, and O. Vitells, "Asymptotic formulae for likelihood-based tests of new physics", *Eur. Phys. J. C* **71** (2011) 1554, doi:10.1140/epjc/s10052-011-1554-0, arXiv:1007.1727. [Erratum: doi:10.1140/epjc/s10052-013-2501-z].